https://doi.org/10.5194/acp-2019-433
Preprint. Discussion started: 1 July 2019

Atmospheric Chemistry and Physics
Discussions

Dynamic shape factor and mixing state of refractory black carbon particles in winter in Beijing using an AAC-DMA-SP2 tandem system

Xiaole PAN[1], Hang LIU[1,2], Yu Wu[3], Yu TIAN[1,2], Yele SUN[1,2,4], Conghui XIE[1,2], Xiaoyong LIU[1,3], Tianhai CHENG[3], Zifa WANG[1,2,4]

[1] State Key Laboratory of Atmospheric Boundary Layer Physics and Atmospheric Chemistry, Institute of Atmospheric Physics, Chinese Academy of Sciences, Beijing, 100029, China

[2] University of Chinese Academy of Sciences, Beijing, 100049, China

[3] State Key Laboratory of Remote Sensing Science, Institute of Remote Sensing and Digital Earth, Chinese Academy of Sciences, No. 20 Datun Road, Beijing 100101, China

[4] Center for Excellence in Regional Atmospheric Environment, Chinese Academy of Science, Xiamen, 361021, China

Correspondence email: panxiaole@mail.iap.ac.cn

Abstract

Refractory black carbon (rBC) is one of the most important short-lived climate forcers in the atmosphere. Light absorption enhancement capacity largely depends on the morphology of rBC-containing particles and their mixing state. In this study, a tandem measuring system, consisting of an aerodynamic aerosol classifier (AAC), a differential mobility analyzer (DMA) and a single particle soot photometer (SP2), was adopted to investigate dynamic shape factor (χ) and its relationship with the mixing state of rBC-containing particles at an urban site of Beijing megacity in winter. The results demonstrated that the aerosol particles with an aerodynamic diameter of 400 ± 1.2 nm normally had a mobility diameter (D_{mob}) ranging from 250 nm to 320 nm, reflecting a large variation in shape under different pollution conditions. Multiple Gaussian fitting on the number mass-equivalent diameter (D_{mev}) distribution of the rBC core determined by SP2 had two peaks at D_{mev} =106.5 nm and D_{mev} =146.3 nm. During pollution episodes, rBC-containing particles tended to have a smaller rBC core than those during clean episodes due to rapid coagulation and condensation processes. The χ values of the particles were found to be ~1.2 during moderate pollution conditions, although the shell-core ratio (S/C) of rBC-containing particles was as high as 2.7 ± 0.3, suggesting that the particles had an irregular structure as a result of the high fraction of nascent rBC aggregates.

https://doi.org/10.5194/acp-2019-433
Preprint. Discussion started: 1 July 2019

Atmospheric Chemistry and Physics Discussions

During heavy pollution episodes, the χ value of the particles was approximately 1.0, indicating that the majority of particles tended to be spherical, and a shell-core model could be reasonable to estimate the light enhancement effect. Considering the variation in shape of the particles, the light absorption enhancement of the particles differed significantly according to the T-matrix model simulation. This study suggested that accurate description of the morphology of rBC-containing particles was crucially important for optical simulation and better evaluation of their climate effect.

https://doi.org/10.5194/acp-2019-433
Preprint. Discussion started: 1 July 2019

Atmospheric Chemistry and Physics Discussions

1. Introduction

It has been well acknowledged that black carbon aerosols play a key role in climate change by disturbing the atmospheric radiation balance on regional and global scales (Bond et al., 2013). First, black carbon aerosol particles can directly absorb downward shortwave solar radiation, heating the atmosphere in the planet boundary layer (PBL), reducing the radiation quantity on the ground, and increasing atmospheric stability (Wang et al., 2018c). It has been reported that black carbon aerosols can suppress the development of the PBL, which facilitates the rapid accumulation of particulate matter (PM) during high pollution episodes (Ding et al., 2016). Many studies in China have pointed out that the interaction between aerosols and meteorology could be attributed to 2-30% of the fast growth of pollution (Wang et al., 2018a;Gao et al., 2015). Second, black carbon aerosols in the atmosphere experience continuous aging processes (coagulation, condensation, oxidation, etc.). As a result, the physical properties of black carbon change from hydrophobic to hydrophilic, which influences their activation capacity to become cloud condensation nuclei (CCN) and consequently influences cloud formation and life span (Laborde et al., 2013;Liu et al., 2013). Black carbon aerosols also contribute to detrimental impacts on human health. These aerosols are normally small with large specific surface areas, and they could be easily inhaled and deposited in the respiratory system with a large fraction of aromatic compounds (such as soot and PAHs). Higher risk of high blood pressure was reported to be related to highway proximity and black carbon emission from cookstoves (Baumgartner et al., 2014).

Black carbon aerosols have different emission sources, such as on-road vehicles, industry, residential activities, and open biomass burning (Zhang et al., 2009). Because black carbon aerosols are mostly produced from incomplete combustion of fossil and biofuel, they are chemically closer to carbon-rich materials consisting of not only carbon nanospheres but also organic matter such as brown carbon (BrC). In practice, mass concentration of black carbon aerosol is operationally determined on the basis of distinct measurement techniques (Lack et al., 2014). For instance, terminology of black carbon normally refers to the light absorbing carbonaceous aerosols that are measured by commercial instruments such as an aethalometer and a multiangle absorption photometer. Another definition, soot, has also been widely used in the combustion research. Soot is normally referred to as refractory black carbon (rBC) and is quantified by a single particle soot photometer on the basis of laser-induced incandescence (LII) emission at a boiling point (Moteki and Kondo, 2007). Not only the mass-equivalent size distribution of rBC but also the mixing state of rBC particles with their host matter could be

https://doi.org/10.5194/acp-2019-433
Preprint. Discussion started: 1 July 2019

Atmospheric Chemistry and Physics Discussions

reasonably estimated according to scattering and incandescent signals. Currently, such a technique is recognized as one of the most reliable for characterizing the microphysical and optical properties of rBC-containing particles. Thus, we adopted rBC terminology in this study.

As mentioned, freshly produced rBC particles are normally hydrophobic and in branch-like structures. These particles are initially externally mixed with other particles (Riemer et al., 2004). With atmospheric aging processes (coagulation, condensation, etc.), the particles gradually mix with other pollutants and become hydrophilic (Zhang et al., 2008). It has been reported that loosely structured rBC aggregates could collapse to compact and spherical aggregates (Adachi et al., 2010). In some cases, rBC particles form a core and become fully encapsulated by their host matter, and consequently, the light-absorbing capacity of rBC-containing particles will enhance significantly due to the "lensing effect" of the coatings. Such absorption enhancement (E_{abs}) has been studied by both Mie theory calculations and observations. Field measurement (Liu et al., 2015) during wintertime in the United Kingdom showed that the E_{abs} value could increase by a factor of up to 2 with increasing coating thickness of the rBC core. In other cases, rBC fractions may be located at the surface or attached to its host material, which results in limited absorption enhancement. For instance, Cappa et al. (2012) reported a small observed E_{abs} value (~6%) on average irrelevant to photochemical aging. Both the above viewpoints have been supported by observational evidence. Liu et al. (2017) pointed out that the absorption enhancement effect is accountable only for a mass ratio of non-rBC to rBC (M_R) greater than 3, and it is very suitable for describing rBC particles from biomass burning sources. Considering the large temporal and spatial variation in emissions, pollution level and meteorological conditions, the mixing state of rBC-containing particles was unevenly distributed from region to region. Therefore, assuming a simplified mixing state and/or E_{abs} value would result in large uncertainty in evaluation of the rBC climate effect.

The morphology of particles changes significantly during atmospheric processing (Zhang et al., 2008). An aggregate model showed that E_{abs} of rBC-containing particles was constrained by the particle morphology with a maximum of ~3.5, even though the M_R value was larger than 10 (Wu et al., 2018). For fresh rBC aggregates, laser-induced incandescence and scattering signals are more sensitive to fractal dimension (He et al., 2015) and monomer polydispersity (Wu et al., 2015) due to the conductive cooling effect (Bambha and Michelsen, 2015). For measurement, quantification of morphological characteristics of rBC-containing particles is labor intensive from the observation on the basis of transmission electron microscopy and discrete dipole approximation (Adachi et al., 2010). Alternatively, the dynamic shape factor (χ)

https://doi.org/10.5194/acp-2019-433
Preprint. Discussion started: 1 July 2019

is an applicable parameter describing the morphological effects of a nonspherical particle in the flow. χ was defined by (Fuchs et al., 1965) as the ratio of actual drag force on the particle to that on an ideal ball with the same volume equivalent diameter. For a spherical particle, the χ value is almost equal to 1.0. The more irregular the particle, the greater the χ value is. In practice, the χ value can be reasonably estimated using a tandem observation system consisting of an aerodynamic aerosol classifier (AAC) and a differential mobility analyzer (DMA). An AAC can select a narrow range of monodispersed aerosol with a known aerodynamic diameter (D_{ae}) that is defined as the diameter of a sphere with a density of 1.0 g/cm^3 that settles at the same terminal velocity as an irregular particle. DMA was used to select the particles with known electrical mobility diameter (D_{mob}), which is defined as the diameter of a sphere that has the same drift velocity in an electric field as an irregular particle. Both the parameters were affected by the shape of the particles.

A tandem observational system consisting of AAC-DMA and SP2 can provide helpful information in estimating the mixing state of rBC-containing particles. However, few studies have been reported in China. The aim of this study is to investigate the variations in the dynamic shape factor of aerosol particles during pollution processes in winter in an urban environment, and the relationship between the morphology of particles and the mixing state of rBC-containing particles, chemical compositions and formation scheme are discussed. The field measurement was performed at the observation field of the State Key Laboratory of Atmospheric Boundary Layer Physics and Atmospheric Chemistry (LAPC) in the Institute of Atmospheric Physics, Chinese Academy of Sciences. The AAC-DMA-SP2 tandem measuring system was placed in an air-conditioned container. Detailed information of the observation site and sampling system have been described in the literature (Pan et al., 2019).

2. Experimental design and method

2.1 Instruments

2.1.1 Single Particle Soot Photometer (SP2)

In this study, the mass size distribution of rBC particles was determined by a single particle soot photometer (SP2, Droplet Measurement Technologies Inc. USA). The principle of SP2 has been described at length in the literature (Schwarz et al., 2008;Moteki and Kondo, 2007;Gao et al., 2007). Briefly, when a rBC particle is passing through a continuous intracavity Nd:YAG laser beam (1064 nm, TEM00 mode), rBC, as a black body, continuously absorbs

https://doi.org/10.5194/acp-2019-433
Preprint. Discussion started: 1 July 2019

energy and eventually emits incandescence at its boiling point (~4000 K). Because peak height of the incandescent signal is approximately linearly proportional to the total mass of the rBC fraction, the mass size distribution of rBC could be obtained presuming a spherical structure and density. In most ambient circumstance, rBC particles are mostly encapsulated or engulfed by other non-refractory matter, and rBC needs more time to evaporate the coating matter before reaching its boiling point. Therefore, the delay time in the occurrence of the peak of the incandescent signal and scattering signal (Δt) is sometimes adopted as a measure to quantify the coating thickness of a rBC-containing particle in many studies (Sedlacek et al., 2012;Huang et al., 2011). A positive value of Δt indicates that the rBC particle is in an internally mixed state, and a negative value indicates the rBC particle might be externally mixed or attached to its host matter.

The SP2 was calibrated before the experiment according to well-established procedures (Miyakawa et al., 2017;Pan et al., 2017). Aquadag aerosols (Lot #9627, Acheson Inc., USA) were used as a calibration standard for the SP2. We adopted an atomizer (model 3072, TSI Inc, USA) and a diffusion dryer and a differential mobility analyzer (DMA; Model 3081, TSI Inc., USA) to prepare the monodispersed Aquadag aerosols, and then the mass of particles (0.5-22 fg) was precisely selected by a centrifugal particle mass analyzer (CPMA, Cambustion Ltd. UK). Note that SP2 was apparently 20~40% more sensitive to Aquadag aerosol than to other rBC types (e.g., fullerene and diesel exhaust). To avoid overestimation resulting from the Aquadag-based calibration curve (Laborde et al., 2012), we corrected the broadband incandescent signal of SP2 with a scaling factor of 0.75. Mass equivalent diameter (D_{mev}) of rBC was calculated assuming a density of 1.8 g cm^{-3} and an ideally spherical structure. During the observation period, the laser power was stable at 4.8 within ±5% at a laser current of 1950 mA, indicating that detection of the rBC size was reliable. Detection efficiency of SP2 was determined to be 0.95-1.05 for the rBC particle with D_{mev} at 80-200 nm. Total uncertainty of the D_{mev} was estimated to be less than 10%.

The scattering signal of SP2 was calibrated using commercially produced polystyrene latex spheres (PSL, Nanosphere Size Standards, Duke Scientific Corp., USA.) with sizes of 203 nm (Lot #185856), 303 nm (Lot #189903), and 400 nm (Lot #189904). Sizes of pure scattering particles or non-rBC matter were determined according to a calibration curve with a prefixed refractive index of 1.48-0i.

2.1.1 Aerodynamic Aerosol Classifier (AAC)

https://doi.org/10.5194/acp-2019-433
Preprint. Discussion started: 1 July 2019

In this study, the particles with known aerodynamic diameter (D_{ae}) were precisely selected with an aerodynamic aerosol classifier (AAC, Cambustion Ltd., UK). The AAC was designed for generating truly monodispersed aerosols with known D_{ae} between 25 nm and 5 µm on the basis of particle relaxation time (τ) that describes the motion of the particle in a shear flow, which is dependent upon instrumental setups such as classifier dimensions, rotating speed, sheath flow, air viscosity and mean free path. The AAC consists of two concentric cylinders rotating at the same direction and rotational speed. Once the aerosols enter the sheath flow through a slit in the inner cylinder wall, the particles experience both a centrifugal force and drag force in the radial direction. Only a particle with a proper τ value can exit with the sampling flow, while the particles with larger τ values adhere to the outer cylinder and particles with smaller τ values exit the classifier with the exhaust flow. Since a charger or neutralizer was not adopted, transmission efficiency of the AAC is higher than 80% for D_{ae} between 200 and 1000 nm. A detailed description of the operation and transfer function is in the literature (Tavakoli and Olfert, 2013). In principle, the aerodynamic diameter D_{ae} and physical characteristics of the AAC in a balanced flow are expressed as the following formula:

$$\frac{C_c(D_{ae})\rho_0 D_{ae}^2}{18\,\mu} = \frac{2Q_{sh}}{\pi\omega^2(r_1+r_2)^2L} \quad (1)$$

where µ is the viscosity of the gas, C_c is the Cunningham slip correction factor, and ρ_0 is the standard density of a particle (1000 kg/m^3). On the right side, Q_{sh} is sheath flow of particle-free air, ω, r_1 and r_2 are the rotational speed and the radius of the inner and outer cylinders, respectively, and L is the distance between the two slits through which the particle enters and leaves the classifier.

2.2 Tandem system setup

A schematic flow chart of the experimental setup is illustrated in Figure 1. As shown, polydispersed aerosols were drawn through a $PM_{2.5}$ cyclone (URG-2000-30EN) at a flow rate of 10 lpm by a supporting pump. The sampling flow was dried by passing through a Nafion dryer (MD-700-24S, TSI) at a flow rate of 0.4 lpm. During the experiment, the AAC was used to select monodispersed particles with a fixed D_{ae} at 400 nm at a constant setpoint (R_s = 5). Then, the sampling aerosols were introduced into the DMA to identify their mobility size

https://doi.org/10.5194/acp-2019-433
Preprint. Discussion started: 1 July 2019

distribution at a scanning mode, and the concentrations of total particles and rBC-containing particles were concurrently measured with a condensation particle counter (Model 3775, TSI) and SP2. As an electrostatic classifier, DMA normally produces monodispersed aerosol with multiple charging artifacts. To avoid such a problem, the scanning D_{mob} range of the DMA was set between 150 and 400 nm, in which there was a distinct singly charged peak with negligible doubly charged particles.

2.3 Methods

2.3.1 Dynamic shape factor

The dynamic shape factor (χ) is theoretically defined as the ratio of the actual drag on the particle to the drag on a sphere of equivalent volume at the same velocity (Fuchs et al., 1965), as follows,

$$\chi = \frac{F_{\mathrm{D}}}{F_{\mathrm{D,ve}}} \tag{2}$$

$$F_{\mathrm{D}} = \frac{3\pi\mu v\chi D_{\mathrm{ve}}}{C_{\mathrm{c}}(D_{\mathrm{ve}})} \tag{3}$$

where F_{D} and $F_{\mathrm{D,ve}}$ are the drag force on a non-spherical particle and its volume equivalent sphere, v is the velocity of the particle with respect to the gas, D_{ve} is the volume equivalent diameter defined as the diameter at which the non-spherical particle was melted to form a droplet while internal void spaces were preserved. The χ value is always larger than one.

For a non-spherical particle that is migrating at a steady velocity in an electric field, its electrical mobility is the same as that of a spherical particle; therefore, we can infer that,

$$\frac{C_{\mathrm{c}}(D_{\mathrm{ve}})}{D_{\mathrm{ve}}\chi} = \frac{C_{\mathrm{c}}(D_{mob})}{D_{mob}} \tag{4}$$

In addition, D_{ae} is defined as the diameter of a spherical particle with a unit density having the same settling velocity (V_{TS}) as the irregular particles under consideration. The equation is given below:

https://doi.org/10.5194/acp-2019-433
Preprint. Discussion started: 1 July 2019

$$v_{TS} = \frac{\rho_P C_c(D_{ve}) D_{ve}^2}{18\mu\chi} = \frac{\rho_0 C_c(D_{ae}) D_{ae}^2}{18\mu} \quad (5)$$

where ρ_P is the density of a particle with internal voids, and we can obtain that,

$$D_{ae} = D_{ve}\sqrt{\frac{\rho_P C_c(D_{ve})}{\chi\rho_0 C_c(D_{ae})}} \quad (6)$$

Among equations (4) and (6), D_{ae} and D_{mob} of the particles were directly measured by the AAC and DMA by solving the equation (Farzan Tavakoli and Jason S. Olfert, 2014), and the D_{ve} and χ values can be obtained as follows,

$$D_{ve} = \sqrt[3]{\frac{D_{ae}^2 \, D_{mob} C_c(D_{ae})\rho_0}{\rho_P \, C_c(D_{mob})}} \quad (7)$$

$$\chi = \frac{C_c(D_{ve}) \, D_{mob}}{C_c(D_{mob}) \, D_{ve}} \quad (8)$$

In this study, the shell-to-core ratio (S/C) of the rBC-containing particles was calculated as follows,

$$S/C = \frac{D_{ve}}{D_{mev,BC}} \; or \; \frac{D_{mob}}{D_{mev,BC}} \quad (9)$$

2.3.1 Effective density

In this study, effective density (ρ_{eff}) of a particle was derived on the basis of the common definition (shown in equation (10)), where the mass of a particle was divided by its volume, the latter of which was calculated using measured D_{mob} presuming the particle was spherical.

$$\rho_{eff} = \frac{6\,m}{\pi\,D_{mob}^3} \quad (10)$$

https://doi.org/10.5194/acp-2019-433
Preprint. Discussion started: 1 July 2019

Here, the mass of the particle was obtained according to the AAC measurement, where the relaxation time of a particle (τ) equals the mass of the particle (m) multiplied by its mobility (B), as shown in equation (11).

$$\tau = B * m \qquad (11)$$

where B and m were calculated according to equations (12) and (13)

$$B = \frac{C_c(D_{\mathrm{mob}})}{3\,\pi\mu\,D_{\mathrm{mob}}} \qquad (12)$$

$$\tau = \frac{C_c(D_{\mathrm{ae}})\rho_0 D_{\mathrm{ae}}^2}{18\,\mu} \qquad (13)$$

Since the D_{mob} was directly measured, ρ_{eff} depends on both the size and shape of the particle. It was for non-spherical particles that the external physical morphology of the particles played a key role in determining ρ_{eff}, not internal voids in the particle.

3. Result and discussion

3.1 Laboratory test of the tandem system

The reliability of the tandem system was verified using both PSL and Aquadag particles. We first used an AAC to choose monodispersed PSL particles with D_{ae} = 210, 315 and 415 nm, and their corresponding mobility size distributions were scanned by a SMPS. We found that the mobility size distributions of all three tested particles show a perfect Gaussian distribution with mode D_{mob} values of 197.8, 304.1 and 396.9 nm. Effective density of the PSL particles was determined by the AAC-DMA system at 1.08–1.12 g/cm^3, approximately 3–6% higher than material density (1.05 g/cm^3), as shown in Figure 2. Our result was consistent with the experiment using DOS (Bis-2-ethylhexyl sebacate) aerosol by (Irwin et al., 2018). For Aquadag particles, To avoid fragmentation of Aquadag particle clusters at dramatic motion in the high-speed rotating cylinder of the AAC, a DMA-AAC tandem experiment was tested. We found that the peak values of the size distribution of D_{ae} were 159.7, 195.5, 232.2, 258.7, 289.4 and 437.8 nm for the particles with D_{mob} = 200, 250, 300, 350, 400 and 602 nm, respectively. Their effective densities were calculated to be 0.724, 0.691, 0.669, 0.615, 0.587 and 0.572

https://doi.org/10.5194/acp-2019-433
Preprint. Discussion started: 1 July 2019

g/cm^3, respectively, in good consistency with the calibration results via mass-mobility methods (mass of the particle was measured by an aerosol particle mass analyzer or centrifugal particle mass analyzer), as shown in SF.1.

3.2 Temporal variations in size distribution

Measurement of the mixing state of the rBC-containing particles using the AAC-DMA-SP2 tandem system was performed from November 27 to December 3 and from December 10 to 14, 2018. Figure 3 depicts the temporal variation in the size distribution of D_{mob} for particles with D_{ae} = 400 nm, a corresponding D_{mev} of rBC particles, mass concentrations of inorganic and organic compositions in PM_1, and dynamic shape factor (χ). The size distribution of particles showed a dominant peak at D_{mob} = 291.6 nm and two small peaks at D_{mob} = 193.3 nm and D_{mob} = 150 nm, as shown in Figure 3a and SF.2. The two small peaks were related to negligible doubly and triply charged particles that only accounted for 1.3% of the total particles. The first peak was attributed to the particle of interest. We can see in Figure 3a and 3e that D_{mob} varied from 250 nm to 350 nm, with a small size (291 ± 8 nm) during heavy pollution (mass concentration of $PM_{2.5}$ > 150 μg/m^3) and clean periods ($PM_{2.5}$ < 35 μg/m^3) and a relatively larger size (316 ± 15 nm) during the moderate pollution period (75 < $PM_{2.5}$ > 150 μg/m^3).

The size distribution of D_{mev} of the rBC particles as a function of time is shown in Figure 3b and 3f. In general, D_{mev} of the rBC particles was 142.8 ± 46.4 nm on average with a large variability between 100 and 200 nm. During the moderate pollution period, D_{mev} of the rBC particles was obviously larger than that during the heavy pollution period. Multiple Gaussian fitting of the size distribution of D_{mev} of the rBC particles during the whole observational period had two peaks at D_{mev} = 106.5 and D_{mev} = 146.3 nm (Figure 4). As expected, the particles during the heavy pollution period had a smaller rBC core because the high concentration of non-rBC matter (sulfate, nitrate, organic carbon, etc.) gave the nascent rBC particles more chance to grow rapidly to larger sizes via both coagulation and condensation processes. Nevertheless, during the moderate pollution period aggregation of rBC particles might play a vital role in growth of rBC clusters, which resulted in larger rBC cores in rBC-containing particles. Figure 3c and 3g show the mass concentrations of chemical composition measured by a high-resolution time-of-flight aerosol mass spectrometer (HR-Tof-AMS). As shown, small D_{mev} of the rBC particles was always companied by a high concentration of $PM_{2.5}$, in particular nitrate. However, D_{mev} of rBC particles was scattered in a larger size range when organic matter was dominant. It is suggested that water-soluble inorganic matter plays a key role in forming a small, compact rBC core.

3.3 Dynamic shape factor

During the observation period, the χ values varied between 1.0 and 1.2, as shown in Figure 3d and 3h. A previous study (Hinds, 1999) pointed out that the χ value for flow in the continuum regime was found to be ~1.08 for cubic particles, ~1.12 for a 2-sphere cluster, and ~1.17 for a compact 4-sphere cluster. Zhang et al. (2016) reported a higher χ value of 1.4–2.0 for In-BC cores with D_{mob} = 150–200 nm during summer at a suburban site in the Beijing megacity. As a matter of fact, fresher rBC-containing particles normally had a larger χ value because of irregularity of the rBC core. Laboratory calibration in this study indicated that Aquadag aerosol had χ values between 1.35 and 1.96 for a D_{mob} between 200 and 602 nm. For the ambient particles with D_{ae} = 400 nm, we found that the χ value had an obviously negative correlation with the mass ratio of inorganic compounds (sum of sulfate, nitrate and ammonium) to organic matter ($MR_{\mathrm{inorg\text{-}to\text{-}org}}$). During the pollution period, the χ value was found to be 1.01 ± 0.01 on average, with a $MR_{\mathrm{inorg\text{-}to\text{-}org}}$ of 1.7 ± 0.8, reflecting that the particles were mostly spherical in shape. However, the χ value increased up to 1.09 ± 0.03 on average, with a $MR_{\mathrm{inorg\text{-}to\text{-}org}}$ of 0.8 ± 0.6, during the clean and moderate pollution periods. Meanwhile, we noticed that relative humidity during the pollution period was apparently higher than that during the other periods. This result implied that the mass fraction of inorganic matter and its hydrophilic processes played an important role in forming spherical particles. Diurnal variation in χ values generally showed a moderate night-high and day-low pattern (Figure 5). The more irregular particles at night were mostly due to high atmospheric loading of primary particles and their coagulation processes (Riemer et al., 2004;Chen et al., 2017). Furthermore, transport of heavy-duty diesel vehicles in the city area also contributed a large amount of irregular soot particles. At noon, the decreases in χ value was mainly related to photochemical processes on the surface of particles, as suggested in (Moffet and Prather, 2009).

3.4 Mixing characteristic of rBC-containing particles

Temporal variation in the S/C ratio of rBC-containing particles calculated on the basis of both D_{mob} (marked as S/C$_{\mathrm{Dmob}}$) and D_{ve} (marked as S/C$_{\mathrm{Dve}}$) are shown in Figure 6a and 6c. We can see that measured S/C$_{\mathrm{Dmob}}$ was consistent with derived S/C$_{\mathrm{Dve}}$ during the heavy pollution period with a mean value of 2.7 ± 0.3 (SF. 3). Since D_{ve} is defined as the diameter of a particle that is

https://doi.org/10.5194/acp-2019-433
Preprint. Discussion started: 1 July 2019

melted to form a droplet while preserving any internal voids (Decarlo et al., 2004), it was always smaller than D_{mob} for irregular particles and the same as that for spherical particles. In this study, the good consistency between D_{mob} and D_{ve} during the heavy pollution period indicated that the particles with D_{ae} = 400 nm were mostly spherical, and a high S/C ratio implied that most of the rBC particles were capsulated by host matter and were in a core-shell configuration as a whole. During the moderate pollution and clean periods, S/C_{Dve} was 2.2 ± 0.6 on average, ~10% smaller than S/C_{Dmob}. This result implied that the particles were irregular, consistent with the analysis of χ.

The distribution of the Δt values of the rBC-containing particles during the observation period is shown in Figure 6b and 6d. We found that the mode Δt value was constant at ~2.6 µs with a relatively larger variability during the clean period, consistent with the multiple Gaussian fitting of the histogram of Δt values (SF.4). As mentioned in Figure 4, D_{mev} of the rBC core during the moderate pollution period was 37% larger than that during the heavy pollution period; however, they had the same Δt value, which indicated that the solo delay time-based analysis might overestimate the coating thickness of rBC-containing particles, though many studies have reported large difference in Δt values for rBC measured at urban pollution (Subramanian et al., 2010;Moteki et al., 2007;Zhang et al., 2018), biomass burning plumes (Pan et al., 2017) and remote marine regions (Taketani et al., 2016). For instance, Moteki and Kondo (2007) found that Δt values of rBC-containing particles from urban areas increased evidently with their aging time, and they classified the thinly coated and thickly coated rBC-containing particles with an experimental threshold Δt value of ~2 µs. Some other studies (Zhang et al., 2018) used a threshold value of 1.6 µs. In some circumstance, there was no distinguished Δt dividing point, which made the classification obscure. For example, a biomass burning experiment (Pan et al., 2017) showed that freshly emitted rBC-containing particles only had one dominant peak, and an S/C ratio of 1.34 corresponded to a higher Δt value of ~3.2 µs. As a matter of fact, the Δt value of rBC-containing particles had no linear relationship with coating thickness and depended on a variety of factors, such as material composition, morphology, voidage, structure of rBC monomers, and compactness of the particle. Laboratory experiments with a glycerol-coated graphite particle showed that the Δt value had a jumping increase from ~1 µs to ~4 µs as the S/C ratio increased to 2, and it decreased gradually with a further increase in the S/C ratio. The jumping time and magnitude depended on the size of the graphite core (Moteki and Kondo, 2007). Bambha and Michelsen (2015) pointed out that the aggregate size and morphology of rBC had a strong influence on the competition between

https://doi.org/10.5194/acp-2019-433
Preprint. Discussion started: 1 July 2019

conductive cooling and absorption heating, which finally affected incandescent and scattering signals and the corresponding Δt value. In this study, we speculated that the irregularity of the particles resulted in a much later occurrence of the incandescent peak (or larger Δt value), albeit their rBC core was larger.

3.5 Influence of rBC on the χ value

The dependence of the χ value as a function of the S/C ratio for rBC-containing particles is shown in Figure 7. A decreasing tendency of the χ value with an increase in the S/C ratio was observed. A power function fitting indicated an S/C ratio of ~3 was a threshold point for rBC-containing particles with D_{ae} = 400 nm. When the S/C ratio was less than 2, the irregularity of rBC-containing particles increased significantly, whereas the particles tended to be spherical when the S/C ratio was larger than 3. Note that a thick coating did not mean that the rBC core was compact and situated in the center of the host matter because the D_{mob} and D_{mev} in this study were measured by different instruments. Our result was generally consistent with a laboratory experiment (Xue et al., 2009), which showed that the χ value of fresh soot was 2.2–4.7. The authors also pointed out that coating of the soot aggregates with organic acid decreased χ because external voids as a result of irregularities were filled by condensed matter. Field observation in Beijing (Zhang et al., 2016) on the χ of rBC cores showed a similar decreasing tendency, and mixing of non-refractory matter evidently reduced the irregularity of the rBC core. Liu et al. (2017) found that the rBC-containing particle could be treated as an internally mixed sphere when its M_R was larger than 3. In this study, M_R of the rBC-containing particle was estimated to be ~6.4; however, variation in the χ value indicated that the rBC particles during the moderate pollution period were not spherical, although the rBC core might have been fully encapsulated by the coating matter. Therefore, a Mie-theory simulation based on a perfect shell-core structure might also result in large uncertainty. Dependence of the χ value of rBC-containing particles on its number fraction in total particles (NF_{rBC}) detected by SP2 (SF. 5) indicated that the χ value of rBC particles increased exponentially with their number fraction, implying that the majority of fresh rBC particles were irregular in shape, particularly during moderate pollution conditions when the mass fraction of the rBC particles in PM_1 was normally higher than 10%.

3.6 Effective density

https://doi.org/10.5194/acp-2019-433
Preprint. Discussion started: 1 July 2019

Effective density (ρ_{eff}) of irregular particles was calculated based on equation (10). In this study, ρ_{eff} values of particles with D_{ae} = 400 nm were found to be 1.71 ± 0.05 g/cm^3 during the heavy pollution period, apparently higher than that (1.56 ± 0.15 g/cm^3) during the moderate pollution period when a substantial amount of irregular particles existed. Our results were generally consistent with mass-mobility-based measurements (~1.5 g/cm^3) in polluted urban environments (Qiao et al., 2018;Zhang et al., 2016), but obviously higher than those in the experiments on nascent particles emitted from gasoline engines (Momenimovahed and Olfert, 2015) and diesel engines (Rissler et al., 2013), fresh soot particles from a propane-fuel burner (Zhang et al., 2008;Xue et al., 2009;Tavakoli and Olfert, 2014), and field observations in a near-traffic urban environment in Denmark (Rissler et al., 2014). A brief summary of the literature is shown in Table 1. In general, ρ_{eff} of particles decreases with increasing D_{mob} and irregularity of the particles. Take nascent particles from vehicle engines for example, the ρ_{eff} value was reported to be less than 1.0 g/cm^3, and it could decrease to as low as 0.4 g/cm^3 when D_{mob} is larger than 300 nm. Fractional dimension (D_f, describing the sphericity of a particles) was inherently relevant to ρ_{eff} of a particle, and they were reported to be 2, 2.17 and 3 for a plane, typical soot particles and a sphere ball, respectively. Laboratory experiments (Zhang et al., 2008) demonstrated that a particle with a smaller D_f value tended to have a faster decreasing tendency of ρ_{eff} because of its irregularity. Note that irregular nascent soot particles would shrink to compact particles once they were exposed to low concentrations of sulfuric acid and a water environment. Consequently, ρ_{eff} of rBC-containing particles might increase as atmospheric aging processes. As a matter of fact, soot agglomerate with a larger D_{mob} experienced a greater degree of collapse due to the uptake effect in the polluted environment, whereas the smaller soot particles acquired a larger sticky chemical mass fraction to cause restructuring.

In a traffic-dominant environment, ρ_{eff} of ambient particles determined based on the mass-mobility method as a function of D_{mob} showed a similar trend with the laboratory studies of diesel-engine exhaust emission (Rissler et al., 2013). In this study, ρ_{eff} of particles with D_{ae} = 400 nm decreased obviously with increasing NF_{rBC}. According to linear fitting (SF. 6), ρ_{eff} of the rBC-containing particles with a C/S ratio = 2.7 was estimated to be ~1.48 g/cm^3, similar to the observation (1.24–1.46 g/cm^3) for the particles with a volatile mass fraction larger than 80% (defined as dense particle in the reference) and much higher than that (0.3–0.4 g/cm^3) for traffic-related fresh soot aggregates. It is suggested that the rBC particles in the urban site of

Beijing megacity might be coated rapidly owing to high atmospheric loading of chemical compositions such as sulfate, nitrate and semivolatile organics.

4. Discussion and atmospheric implication

Quantification climate effect of rBC-containing particles has large uncertainty due to their extremely complex morphology and coexisting chemical compositions. In an urban environment, intensive emission of rBC particles was due to anthropogenic activities, such as transport of on-road vehicles, house cooking, and waste incineration. The characteristics of the mixing state of rBC-containing particles was reported to be distinguished differently region by region. For instance, rBC particles observed in a developed metropolis were reported to present as aggregation monomers, which had loose fractal structures, that were easily classified as nascent. In Beijing, we found that rBC particles always had thick coatings mostly owing to rapid mixing with high concentrations of other chemical compositions. (Peng et al., 2016) pointed out the rBC aging exhibited two distinct stages with an initial destruction of rBC particles from a fractal to spherical morphology and subsequent growth process at which a fully compact core-shell configuration was formed, and even the time scale of such a transformation was fast (less than ~4.6 hours). From the viewpoint of this study, we suggested that these two processes would happen simultaneously, and rBC-containing particles with D_{mev} = 100–150 nm were irregular in shape, even though the rBC core was thickly coated or encapsulated by the host composition. Spherical rBC-containing particles would be a true case only when high mass concentration of water soluble matter and high relative humidity conditions were fulfilled, and interaction with water vapor on the surface of rBC-containing particles would ultimately change the irregularity, as archived in both observations (Zhang et al., 2008) and modeling studies (Fan et al., 2016).

A proper parameterization for the mixing state of rBC-containing particles was essential for evaluating its optical properties. In this study, we found that the overall morphology of rBC-containing particles was still irregular even when the S/C ratio was high. Herein, the morphologies of rBC-containing particles were constructed and integrated by a novel aggregate model and their random-orientation scattering cross-sections of particles were simulated on the basis of a superposition T-matrix method by solving Maxwell's equations numerically. Three sensitive simulations were conducted. (I) Freshly emitted rBC particles were treated as a branched agglomerate with hundreds of small spherical primary particles. (II) Thinly coated rBC particles were simulated by the aggregation of core-shell monomers (Wu et al., 2014). (III)

Thickly coated rBC particles were in a core-shell configuration with an aggregated rBC core heavily coated by large non-rBC particles, and all rBC monomers were inside of the non-rBC particle (Cheng et al., 2014). D_f were applied for indicating the compactness of fractal aggregated BC particles. In the simulations, the values of D_f were varied from 2 to 3 with a fractal prefactor of 1.2, corresponding to the rBC aggregates with loose to compact structures. The mean diameters of rBC monomers were assumed to be 0.04 μm, and monomer numbers of the individual aggregates were obtained by volume-equivalent diameter of pure rBC components. The results showed that the variability in optical properties of thinly coated rBC particles (I) were more significant than that of simulations of II and III, up to ~60% (mass scattering cross-section, MSC) and ~30% (for mass absorption cross-section, MAC), especially for the cases with small D_f. When the fractal aggregated rBC particles are heavily coated with non-rBC particles, these diversities were weakened with ~10% variability for MAC. These variations were mainly dependent on the growing contributions of non-rBC components and the more compact morphologies of rBC aggregates. It is suggested to include the complex particle morphology in the optical simulations of rBC-containing aerosols.

Recently, Liu et al. (2017) indicated that the ratio of the observed scattering cross-section of rBC-containing particles to that of the Mie-theory simulation based on the simplified core-shell model ($S_{meas.}/S_{model}$) decreased evidently as M_R increased, and $S_{meas.}/S_{model}$ tended to be ~1 when M_R was larger than ~3. The maximum discrepancy occurred at $1 < M_R < 2$, indicating that mixing state of rBC-containing particles was more complicated at the initial timing of the coating stage. Wu et al. (2018) pointed out that the simulation errors were mainly caused by morphological simplification of the rBC-containing particles, although dramatic morphological alteration and destruction of the rBC core occurred (China et al., 2013;Adachi et al., 2010). This study provided direct evidence that the rBC-containing particles might also be irregular in shape even when $M_R > 6$. This study also indicated that delay time analysis of rBC-containing particles would result in large uncertainties in estimating the coating thickness of particles in urban environments because of the more fractal structure of rBC aggregates. Sedlacek et al. (2012) found rBC-containing particles in one biomass burning plume with a clear negative Δt value; however, such a phenomenon was not observed in the laboratory experiment (Pan et al., 2017). More observation studies on the size-selected rBC-containing particles from open burning of biomass with different aging scales were suggested to better manifest its mixing characteristics.

https://doi.org/10.5194/acp-2019-433
Preprint. Discussion started: 1 July 2019

Mass concentrations of $PM_{2.5}$ in both China (Ma et al., 2016) and western Japan (Wang et al., 2017;Uno et al., 2017) were reported to be gradually decreasing recently due to a decrease in SO_2 emission (Wang et al., 2018b). Nevertheless, urban air pollution in China was still serious as a result of intensive anthropogenic activities such as on-road vehicle emission, which included not only rBC particles but also semivolatile organics. As suggested in this study, the nascent rBC particles would experience rapid transformation and reconstruction and simultaneous coating processes. Therefore, measurement-constrained optical modeling of rBC particles from both anthropogenic sources (i.e., transport, open biomass burning) and natural sources (i.e., wild fire) would be helpful in better evaluating their metrological feedbacks and regional environmental effects. In the urban environment, irregular rBC-containing particles normally have very large specific surface areas, and heterogeneous reactions on the surface could influence NOx chemistry (Monge et al., 2010) and further atmospheric oxidants (Guan et al., 2017). Therefore, a joint control on both vehicle ownership and quality of oil products could benefit the campaign against urban pollution.

5. Conclusions

In this study, mixing characteristics and dynamic shape factor of rBC-containing particles with known aerodynamic sizes was investigated at a typical urban site in Beijing megacity using a tandem measuring system consisting of an aerodynamic aerosol classifier (AAC), a differential mobility analyzer (DMA) and a single particle soot photometer (SP2) in winter of 2018. Mass-equivalent size distribution of rBC particles (D_{mev}), delay time (Δt), shell-core ratio (S/C) and its dependence on dynamic shape factor (χ), as well as effective density (ρ_{eff}), were analyzed. We found that in the urban environment, the D_{mev} distribution for the rBC-containing particles with an aerodynamic diameter of 400 ± 0.5 nm had two peaks with a dominant mode value at D_{mev} = 146.3 nm and a small peak at D_{mev} = 106.5 nm, and rBC-containing particles during heavy pollution conditions had a smaller rBC core, implying that the rBC particles easily gained coatings as a result of coagulation and condensation processes with other matter. D_{mob} of particles had an obvious variation ranging from 250.6 nm (heavy pollution period) to 320 nm (moderate pollution period). During the clean period, the χ value of the rBC-containing particles were estimated to be ~1.2, suggesting that the particles were in an irregular structure that was related to the high fraction of fractal rBC particles. During heavy pollution episodes, the χ value of the particles was ~1.0, indicating that the majority of particles tended to be spherical, and a shell-core model could be reasonable to estimate its light enhancement effect. Although the χ value varied obviously, the S/C ratio of rBC-containing particles during the whole observation period had a mean value of 2.7 ± 0.3, indicating the thickly coated rBC particles might also have irregular shapes. Therefore, a spherical shell-core model may also introduce bias for optical simulation. In addition, delay time analysis of the peaks of incandescence and scattering signals showed a stale Δt value of ~2.6 μs, almost irrespective of the shape of the particles due to conductive cooling of external voids, etc. Optical properties of irregular rBC-containing particles were simulated on the basis of a novel aggregate model and a superposition T-matrix method, which indicated that light absorption enhancement of particles differed significantly if morphology of rBC-containing particles was considered. Therefore, an appropriate description of the physical properties of rBC-containing particles such as shape factor was crucially important in evaluating the climate effect.

Data availability. To request SP2 and SMPS data for scientific research purposes, please contact Dr. Xiaole Pan at the Institute of Atmospheric Physics, Chinese Academy of Sciences, via email (panxiaole@mail.iap.ac.cn)

Competing interests. The authors declare that they have no conflicts of interest.

Author contribution. X. P., H. L. and Z. W. designed and conducted the experiment. Y.W. and Y. T. and T. C. performed the model simulation on the optical property of aerosols. Y. S. and C. X conducted observation on chemical compositions of submicron particles using AMS.

Acknowledgements. This research was supported by the National Nature Science Foundation of China (Grant no. 41877314)

References

Adachi, K., Chung, S. H., and Buseck, P. R.: Shapes of soot aerosol particles and implications for their effects on climate, J. Geophys. Res.-Atmos., 115, Artn D1520610.1029/2009jd012868, 2010.

Bambha, R. P., and Michelsen, H. A.: Effects of aggregate morphology and size on laser-induced incandescence and scattering from black carbon (mature soot), J Aerosol Sci, 88, 159-181, 10.1016/j.jaerosci.2015.06.006, 2015.

Baumgartner, J., Zhang, Y., Schauer, J. J., Huang, W., Wang, Y., and Ezzati, M.: Highway proximity and black carbon from cookstoves as a risk factor for higher blood pressure in rural China, Proceedings of the National Academy of Sciences, 111, 13229-13234, 10.1073/pnas.1317176111, 2014.

Bond, T. C., Doherty, S. J., Fahey, D., Forster, P., Berntsen, T., DeAngelo, B., Flanner, M., Ghan, S., Kärcher, B., and Koch, D.: Bounding the role of black carbon in the climate system: A scientific assessment, Journal of Geophysical Research: Atmospheres, 118, 5380-5552, 2013.

https://doi.org/10.5194/acp-2019-433
Preprint. Discussion started: 1 July 2019

Cappa, C. D., Onasch, T. B., Massoli, P., Worsnop, D. R., Bates, T. S., Cross, E. S., Davidovits, P., Hakala, J., Hayden, K. L., Jobson, B. T., Kolesar, K. R., Lack, D. A., Lerner, B. M., Li, S. M., Mellon, D., Nuaaman, I., Olfert, J. S., Petaja, T., Quinn, P. K., Song, C., Subramanian, R., Williams, E. J., and Zaveri, R. A.: Radiative Absorption Enhancements Due to the Mixing State of Atmospheric Black Carbon, Science, 337, 1078-1081, 10.1126/science.1223447, 2012.

Chen, X. S., Wang, Z. F., Yu, F. Q., Pan, X. L., Li, J., Ge, B. Z., Wang, Z., Hu, M., Yang, W. Y., and Chen, H. S.: Estimation of atmospheric aging time of black carbon particles in the polluted atmosphere over central-eastern China using microphysical process analysis in regional chemical transport model, Atmos Environ, 163, 44-56, 10.1016/j.atmosenv.2017.05.016, 2017.

China, S., Mazzoleni, C., Gorkowski, K., Aiken, A. C., and Dubey, M. K.: Morphology and mixing state of individual freshly emitted wildfire carbonaceous particles, Nat Commun, 4, ARTN 2122 10.1038/ncomms3122, 2013.

Decarlo, P., Slowik, J., Worsnop, D., PaulDavidovits, and Jimenez, J.: Particle Morphology and Density Characterization by Combined Mobility and Aerodynamic Diameter Measurements. Part 1: Theory, Aerosol Science & Technology, 38, 1185-1205, 2004.

Ding, A. J., Huang, X., Nie, W., Sun, J. N., Kerminen, V. M., Petäjä, T., Su, H., Cheng, Y. F., Yang, X. Q., and Wang, M. H.: Enhanced haze pollution by black carbon in megacities in China, Geophysical Research Letters, 43, 2016.

Fan, M., Chen, L. F., Li, S. S., Zou, M. M., Su, L., and Tao, J. H.: The Effects of Morphology and Water Coating on the Optical Properties of Soot Aggregates, Aerosol Air Qual Res, 16, 1315-1326, 10.4209/aaqr.2015.04.0250, 2016.

Farzan Tavakoli, Jason S. Olfert: Determination of particle mass, effective density, mass–mobility exponent, and dynamic shape factor using an aerodynamic aerosol classifier and a differential mobility analyzer in tandem, Journal of Aerosol Science, 75 (2014) 35–42, http://dx.doi.org/10.1016/j.jaerosci.2014.04.010

Fuchs, N. A., Daisley, R. E., Fuchs, M., Davies, C. N., and Straumanis, M. E.: The Mechanics of Aerosols, Phys Today, 18, 73-73, 1965.

Gao, R. S., Schwarz, J. P., Kelly, K. K., Fahey, D. W., Watts, L. A., Thompson, T. L., Spackman, J. R., Slowik, J. G., Cross, E. S., Han, J. H., Davidovits, P., Onasch, T. B., and Worsnop, D. R.: A novel method for estimating light-scattering properties of soot aerosols using a modified single-particle soot photometer, Aerosol Science and Technology, 41, 125-135, 10.1080/02786820601118398, 2007.

Gao, Y., Zhang, M., Liu, Z., Wang, L., Wang, P., Xia, X., Tao, M., and Zhu, L.: Modeling the feedback between aerosol and meteorological variables in the atmospheric boundary layer during a severe fog-haze event over the North China Plain, Atmospheric Chemistry and Physics, 15, 4279-4295, 10.5194/acp-15-4279-2015, 2015.

Guan, C., Li, X. L., Zhang, W. G., and Huang, Z.: Identification of Nitration Products during Heterogeneous Reaction of NO2 on Soot in the Dark and under Simulated Sunlight, J Phys Chem A, 121, 482-492, 10.1021/acs.jpca.6b08982, 2017.

He, C., Liou, K. N., Takano, Y., Zhang, R., Zamora, M. L., Yang, P., Li, Q., and Leung, L. R.: Variation of the radiative properties during black carbon aging: theoretical and experimental intercomparison, Atmospheric Chemistry and Physics, 15, 11967-11980, 10.5194/acp-15-11967-2015, 2015.

Hinds, W. C.: Aerosol technology: properties, behavior, and measurement of airborne particles, J Aerosol Sci, 31, 1121-1122, 1999.

Huang, X. F., Gao, R. S., Schwarz, J. P., He, L. Y., Fahey, D. W., Watts, L. A., McComiskey, A., Cooper, O. R., Sun, T. L., Zeng, L. W., Hu, M., and Zhang, Y. H.: Black carbon measurements in the Pearl River Delta region of China, J. Geophys. Res.-Atmos., 116, Artn D12208 10.1029/2010jd014933, 2011.

Irwin, M., Bradley, H., Duckhouse, M., Hammond, M., and Peckham, M. S.: High spatio-temporal resolution pollutant measurements of on-board vehicle emissions using ultra-fast response gas analyzers, Atmos Meas Tech, 11, 3559-3567, 10.5194/amt-11-3559-2018, 2018.

Laborde, M., Mertes, P., Zieger, P., Dommen, J., Baltensperger, U., and Gysel, M.: Sensitivity of the Single Particle Soot Photometer to different black carbon types, Atmos Meas Tech, 5, 1031-1043, 10.5194/amt-5-1031-2012, 2012.

Laborde, M., Crippa, M., Tritscher, T., Juranyi, Z., Decarlo, P. F., Temime-Roussel, B., Marchand, N., Eckhardt, S., Stohl, A., Baltensperger, U., Prevot, A. S. H., Weingartner, E., and Gysel, M.: Black carbon physical properties and mixing state in the European megacity Paris, Atmospheric Chemistry and Physics, 13, 5831-5856, 10.5194/acp-13-5831-2013, 2013.

Lack, D. A., Moosmüller, H., McMeeking, G. R., Chakrabarty, R. K., and Baumgardner, D.: Characterizing elemental, equivalent black, and refractory black carbon aerosol particles: a review of techniques, their limitations and uncertainties, Analytical and bioanalytical chemistry, 406, 99-122, 10.1007/s00216-013-7402-3, 2014.

Liu, D., Allan, J., Whitehead, J., Young, D., Flynn, M., Coe, H., McFiggans, G., Fleming, Z. L., and Bandy, B.: Ambient black carbon particle hygroscopic properties controlled by mixing state and composition, Atmospheric Chemistry and Physics, 13, 2015-2029, 10.5194/acp-13-2015-2013, 2013.

Liu, D. T., Whitehead, J., Alfarra, M. R., Reyes-Villegas, E., Spracklen, D. V., Reddington, C. L., Kong, S. F., Williams, P. I., Ting, Y. C., Haslett, S., Taylor, J. W., Flynn, M. J., Morgan, W. T., McFiggans, G., Coe, H., and Allan, J. D.: Black-carbon absorption enhancement in the atmosphere determined by particle mixing state, Nat Geosci, 10, 184-U132, 10.1038/Ngeo2901, 2017.

Liu, S., Aiken, A. C., Gorkowski, K., Dubey, M. K., Cappa, C. D., Williams, L. R., Herndon, S. C., Massoli, P., Fortner, E. C., Chhabra, P. S., Brooks, W. A., Onasch, T. B., Jayne, J. T., Worsnop, D. R., China, S., Sharma, N., Mazzoleni, C., Xu, L., Ng, N. L., Liu, D., Allan, J. D., Lee, J. D., Fleming, Z. L., Mohr, C., Zotter, P., Szidat, S., and Prevot, A. S. H.: Enhanced light absorption by mixed source black and brown carbon particles in UK winter, Nat Commun, 6, ARTN 843510.1038/ncomms9435, 2015.

Ma, Z. W., Hu, X. F., Sayer, A. M., Levy, R., Zhang, Q., Xue, Y. G., Tong, S. L., Bi, J., Huang, L., and Liu, Y.: Satellite-Based Spatiotemporal Trends in PM2.5 Concentrations: China, 2004-2013, Environ Health Persp, 124, 184-192, 10.1289/ehp.1409481, 2016.

Miyakawa, T., Oshima, N., Taketani, F., Komazaki, Y., Yoshino, A., Takami, A., Kondo, Y., and Kanaya, Y.: Alteration of the size distributions and mixing states of black carbon through transport in the boundary layer in east Asia, Atmospheric Chemistry and Physics, 17, 5851-5864, 10.5194/acp-17-5851-2017, 2017.

Moffet, R. C., and Prather, K. A.: In-situ measurements of the mixing state and optical properties of soot with implications for radiative forcing estimates, P Natl Acad Sci USA, 106, 11872-11877, 10.1073/pnas.0900040106, 2009.

Momenimovahed, A., and Olfert, J. S.: Effective Density and Volatility of Particles Emitted from Gasoline Direct Injection Vehicles and Implications for Particle Mass Measurement, Aerosol Science and Technology, 49, 1051-1062, 10.1080/02786826.2015.1094181, 2015.

Monge, M. E., D'Anna, B., Mazri, L., Giroir-Fendler, A., Ammann, M., Donaldson, D. J., and George, C.: Light changes the atmospheric reactivity of soot, P Natl Acad Sci USA, 107, 6605-6609, 10.1073/pnas.0908341107, 2010.

Moteki, N., and Kondo, Y.: Effects of mixing state on black carbon measurements by laser-induced incandescence, Aerosol Science and Technology, 41, 398-417, 10.1080/02786820701199728, 2007.

Moteki, N., Kondo, Y., Miyazaki, Y., Takegawa, N., Komazaki, Y., Kurata, G., Shirai, T., Blake, D., Miyakawa, T., and Koike, M.: Evolution of mixing state of black carbon particles: Aircraft measurements over the western Pacific in March 2004, Geophysical Research Letters, 34, 2007.

Pan, X. L., Kanaya, Y., Taketani, F., Miyakawa, T., Inomata, S., Komazaki, Y., Tanimoto, H., Wang, Z., Uno, I., and Wang, Z. F.: Emission characteristics of refractory black carbon aerosols from fresh biomass burning: a perspective from laboratory experiments, Atmospheric Chemistry and Physics, 17, 13001-13016, 10.5194/acp-17-13001-2017, 2017.

Pan, X. L., Ge, B. Z., Wang, Z., Tian, Y., Liu, H., Wei, L. F., Yue, S. Y., Uno, I., Kobayashi, H., Nishizawa, T., Shimizu, A., Fu, P. Q., and Wang, Z. F.: Synergistic effect of water-soluble species and relative humidity on morphological changes in aerosol particles in the Beijing megacity during severe pollution episodes, Atmospheric Chemistry and Physics, 19, 219-232, 10.5194/acp-19-219-2019, 2019.

Peng, J. F., Hu, M., Guo, S., Du, Z. F., Zheng, J., Shang, D. J., Zamora, M., Zeng, L. M., Shao, M., Wu, Y. S., Zheng, J., Wang, Y., Glen, C., Collins, D., Molina, M., and Zhang, R. Y.: Markedly enhanced absorption and direct radiative forcing of black carbon under polluted urban environments, Abstr Pap Am Chem S, 252, 2016.

Qiao, K., Wu, Z. J., Pei, X. Y., Liu, Q. Y., Shang, D. J., Zheng, J., Du, Z. F., Zhu, W. F., Wu, Y. S., Lou, S. R., Guo, S., Chan, C. K., Pathak, R. K., Hallquist, M., and Hu, M.: Size-resolved effective density of submicron particles during summertime in the rural atmosphere of Beijing, China, J Environ Sci-China, 73, 69-77, 10.1016/j.jes.2018.01.012, 2018.

Riemer, N., Vogel, H., and Vogel, B.: Soot aging time scales in polluted regions during day and night, Atmospheric Chemistry and Physics, 4, 1885-1893, DOI 10.5194/acp-4-1885-2004, 2004.

Rissler, J., Messing, M. E., Malik, A. I., Nilsson, P. T., Nordin, E. Z., Bohgard, M., Sanati, M., and Pagels, J. H.: Effective Density Characterization of Soot Agglomerates from Various Sources and Comparison to Aggregation Theory, Aerosol Science and Technology, 47, 792-805, 10.1080/02786826.2013.791381, 2013.

Rissler, J., Nordin, E. Z., Eriksson, A. C., Nilsson, P. T., Frosch, M., Sporre, M. K., Wierzbicka, A., Svenningsson, B., Londahl, J., Messing, M. E., Sjogren, S., Hemmingsen, J. G., Loft, S., Pagels, J. H., and Swietlicki, E.: Effective Density and Mixing State of Aerosol Particles in a Near-Traffic Urban Environment, Environ Sci Technol, 48, 6300-6308, 10.1021/es5000353, 2014.

Schwarz, J. P., Gao, R. S., Spackman, J. R., Watts, L. A., Thomson, D. S., Fahey, D. W., Ryerson, T. B., Peischl, J., Holloway, J. S., Trainer, M., Frost, G. J., Baynard, T., Lack, D. A., de Gouw, J. A., Warneke, C., and Del Negro, L. A.: Measurement of the mixing state, mass, and optical size of individual black carbon particles in urban and biomass burning emissions, Geophysical Research Letters, 35, Artn L13810 10.1029/2008gl033968, 2008.

Sedlacek, A. J., Lewis, E. R., Kleinman, L., Xu, J. Z., and Zhang, Q.: Determination of and evidence for non-core-shell structure of particles containing black carbon using the Single-Particle Soot Photometer (SP2), Geophysical Research Letters, 39, 2012.

Subramanian, R., Kok, G. L., Baumgardner, D., Clarke, A., Shinozuka, Y., Campos, T. L., Heizer, C. G., Stephens, B. B., de Foy, B., Voss, P. B., and Zaveri, R. A.: Black carbon over Mexico: the effect of atmospheric transport on mixing state, mass absorption cross-section, and BC/CO ratios, Atmospheric Chemistry and Physics, 10, 219-237, 10.5194/acp-10-219-2010, 2010.

Taketani, F., Miyakawa, T., Takashima, H., Komazaki, Y., Pan, X., Kanaya, Y., and Inoue, J.: Shipborne observations of atmospheric black carbon aerosol particles over the Arctic Ocean, Bering Sea, and North Pacific Ocean during September 2014, J. Geophys. Res.-Atmos., 121, 1914-1921, 10.1002/2015jd023648, 2016.

Tavakoli, F., and Olfert, J. S.: An Instrument for the Classification of Aerosols by Particle Relaxation Time: Theoretical Models of the Aerodynamic Aerosol Classifier, Aerosol Science and Technology, 47, 916-926, 10.1080/02786826.2013.802761, 2013.

Tavakoli, F., and Olfert, J. S.: Determination of particle mass, effective density, mass-mobility exponent, and dynamic shape factor using an aerodynamic aerosol classifier and a differential mobility analyzer in tandem, J Aerosol Sci, 75, 35-42, 10.1016/j.jaerosci.2014.04.010, 2014.

Uno, I., Osada, K., Yumimoto, K., Wang, Z., Itahashi, S., Pan, X. L., Hara, Y., Kanaya, Y., Yamamoto, S., and Fairlie, T. D.: Seasonal variation of fine- and coarse-mode nitrates and related aerosols over East Asia: synergetic observations and chemical transport model analysis, Atmospheric Chemistry and Physics, 17, 14181-14197, 10.5194/acp-17-14181-2017, 2017.

Wang, H., Peng, Y., Zhang, X. Y., Liu, H. L., Zhang, M., Che, H. Z., Cheng, Y. L., and Zheng, Y.: Contributions to the explosive growth of PM2.5 mass due to aerosol-radiation feedback and decrease in turbulent diffusion during a red alert heavy haze in Beijing-Tianjin-Hebei, China, Atmospheric Chemistry and Physics, 18, 17717-17733, 10.5194/acp-18-17717-2018, 2018a.

Wang, T., Wang, P. C., Theys, N., Tong, D., Hendrick, F., Zhang, Q., and Van Roozendael, M.: Spatial and temporal changes in SO2 regimes over China in the recent decade and the driving mechanism, Atmospheric Chemistry and Physics, 18, 18063-18078, 10.5194/acp-18-18063-2018, 2018b.

Wang, Z., Pan, X. L., Uno, I., Li, J., Wang, Z. F., Chen, X. S., Fu, P. Q., Yang, T., Kobayashi, H., Shimizu, A., Sugimoto, N., and Yamamoto, S.: Significant impacts of heterogeneous reactions on the chemical composition and mixing state of dust particles: A case study during dust events over northern China, Atmos Environ, 159, 83-91, 10.1016/j.atmosenv.2017.03.044, 2017.

Wang, Z. L., Huang, X., and Ding, A. J.: Dome effect of black carbon and its key influencing factors: a one-dimensional modelling study, Atmospheric Chemistry and Physics, 18, 2821-2834, 10.5194/acp-18-2821-2018, 2018c.

Wu, Y., Cheng, T. H., Zheng, L. J., Chen, H., and Xu, H.: Single scattering properties of semi-embedded soot morphologies with intersecting and non-intersecting surfaces of absorbing spheres and non-absorbing host, J Quant Spectrosc Ra, 157, 1-13, 10.1016/j.jqsrt.2015.02.006, 2015.

Wu, Y., Cheng, T. H., Liu, D. T., Allan, J. D., Zheng, L. J., and Chen, H.: Light Absorption Enhancement of Black Carbon Aerosol Constrained by Particle Morphology, Environ Sci Technol, 52, 6912-6919, 10.1021/acs.est.8b00636, 2018.

Xue, H. X., Khalizov, A. F., Wang, L., Zheng, J., and Zhang, R. Y.: Effects of Coating of Dicarboxylic Acids on the Mass-Mobility Relationship of Soot Particles, Environ Sci Technol, 43, 2787-2792, 10.1021/es803287v, 2009.

Zhang, Q., Streets, D. G., Carmichael, G. R., He, K. B., Huo, H., Kannari, A., Klimont, Z., Park, I. S., Reddy, S., Fu, J. S., Chen, D., Duan, L., Lei, Y., Wang, L. T., and Yao, Z. L.: Asian emissions in 2006 for the NASA INTEX-B mission, Atmospheric Chemistry and Physics, 9, 5131-5153, DOI 10.5194/acp-9-5131-2009, 2009.

Zhang, R. Y., Khalizov, A. F., Pagels, J., Zhang, D., Xue, H. X., and McMurry, P. H.: Variability in morphology, hygroscopicity, and optical properties of soot aerosols during atmospheric processing, P Natl Acad Sci USA, 105, 10291-10296, 10.1073/pnas.0804860105, 2008.

Zhang, Y. X., Zhang, Q., Cheng, Y. F., Su, H., Kecorius, S., Wang, Z. B., Wu, Z. J., Hu, M., Zhu, T., Wiedensohler, A., and He, K. B.: Measuring the morphology and density of internally mixed black carbon with SP2 and VTDMA: new insight into the absorption enhancement of black carbon in the atmosphere, Atmos Meas Tech, 9, 1833-1843, 10.5194/amt-9-1833-2016, 2016.

Zhang, Y. X., Su, H., Ma, N., Li, G., Kecorius, S., Wang, Z. B., Hu, M., Zhu, T., He, K. B., Wiedensohler, A., Zhang, Q., and Cheng, Y. F.: Sizing of Ambient Particles From a Single-Particle Soot Photometer Measurement to Retrieve Mixing State of Black Carbon at a Regional

https://doi.org/10.5194/acp-2019-433
Preprint. Discussion started: 1 July 2019

Site of the North China Plain, J. Geophys. Res.-Atmos., 123, 12778-12795, 10.1029/2018jd028810, 2018.

https://doi.org/10.5194/acp-2019-433
Preprint. Discussion started: 1 July 2019

Atmospheric Chemistry and Physics
Open Access
EGU
Discussions

Tables

Table 1 Brief summary of effective density measurement in previous studies.

Aerosol type	Measurement system	Particle size, D_{mob} (nm)	Effective density (g/cm^3)	Description	Reference
Ambient particles	DMA+APM	50-350	1.25-1.50	Two peaks were found of effective density distribution. The data was effective density of the second peak.	(Rissler et al., 2014)
	DMA+CPMA	50-350	1.43-1.55	The measurement was conducted in Beijing in summer.	(Qiao et al., 2014)
Soot	DMA+APM	100-300	0.82-0.30	Vehicle exhaust	(Rissler et al., 2013)
	DMA+APM	100-300	0.41-0.18	Flame generated soot	
	DMA+CPMA	50-250	0.77-0.38	Vehicle exhaust	(Momenimovahed et al., 2015)
	DMA+AAC	95-637	0.18-0.86	Generated from an inverted burner	(Frazan et al., 2014)
BC core	DMA+CPMA	50-250	0.68-0.36	Denuded vehicle exhaust	(Momenimovahed et al., 2015)
	DMA+SP2	150-200	0.9-0.5	Denuded ambient rBC	(Zhang et al., 2016)
	DMA+APM	150-200	0.4-0.2	Denuded laboratory soot	(Xue et al., 2009)

https://doi.org/10.5194/acp-2019-433
Preprint. Discussion started: 1 July 2019

Figures

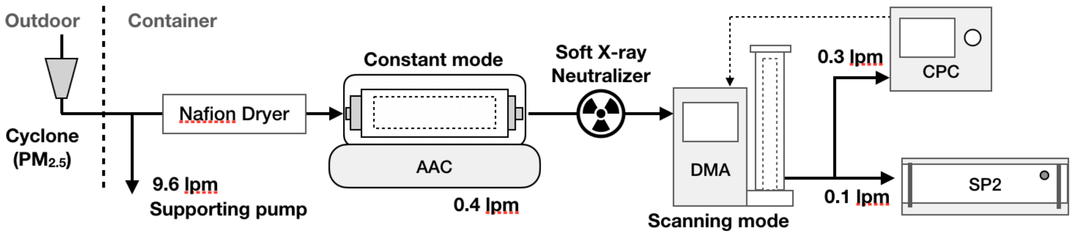

Figure 1 Illustration of the experimental setup of the AAC-DMA-SP2 system.

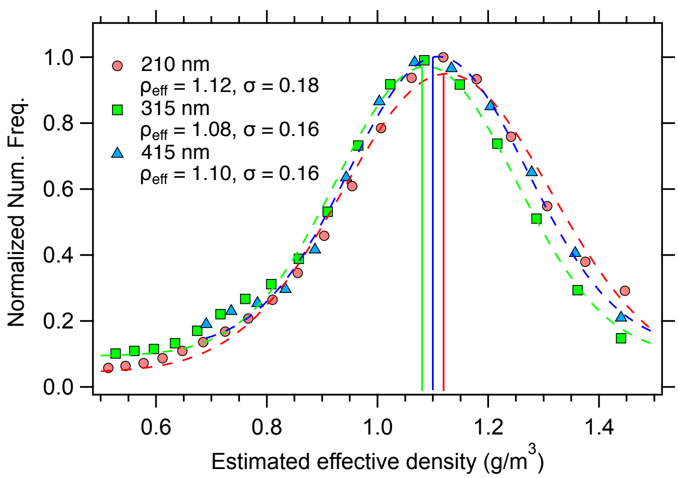

Figure 2 Estimated effective density of PSL particles on the basis of the AAC-DMA tandem system.

https://doi.org/10.5194/acp-2019-433
Preprint. Discussion started: 1 July 2019

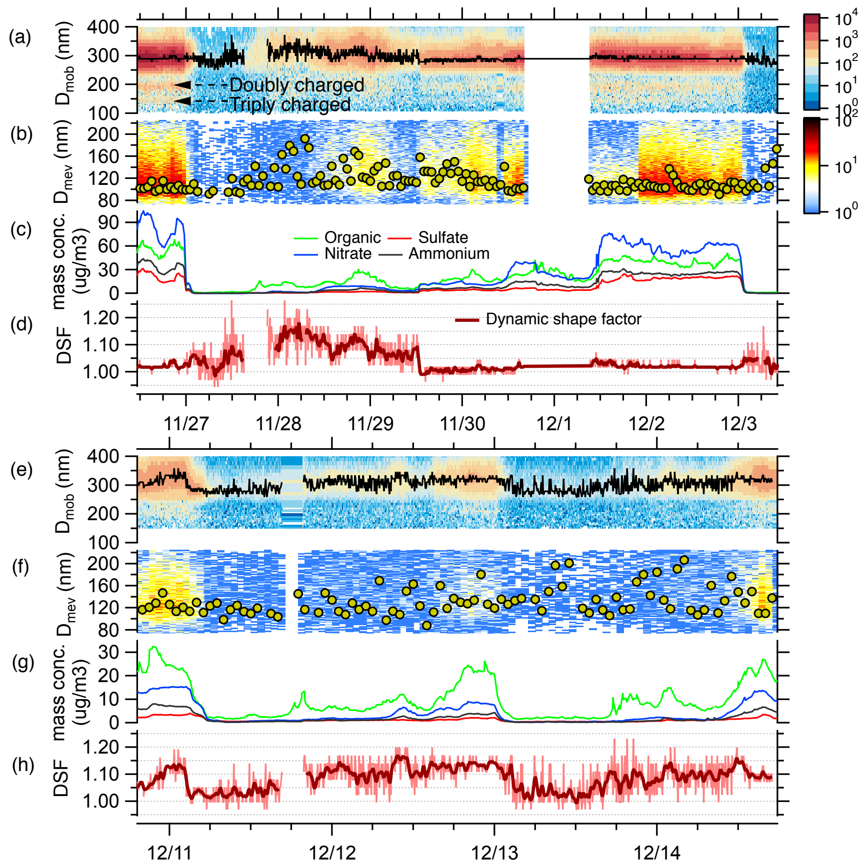

Figure 3 Temporal variations in distribution of D_{mob} (a, e), D_{mev} (b, f), mass concentrations of water soluble composition measured by AMS (c, g), and derived dynamic shape factor (d, h) during the observation periods

https://doi.org/10.5194/acp-2019-433
Preprint. Discussion started: 1 July 2019

Atmospheric Chemistry and Physics Discussions

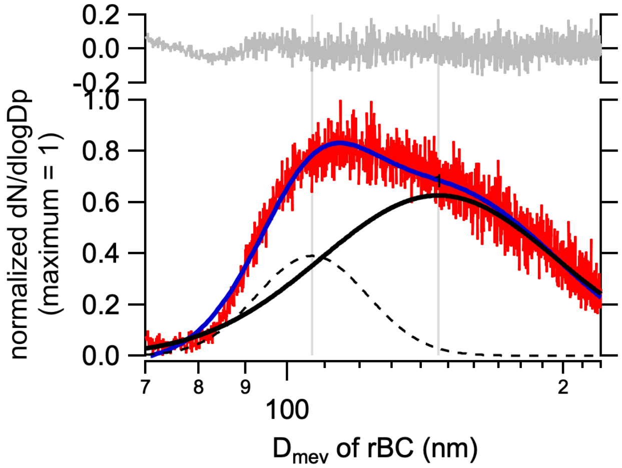

Figure 4 Normalized size distribution of D_{mev} of rBC particles and multi-Gaussian fitting results.

https://doi.org/10.5194/acp-2019-433
Preprint. Discussion started: 1 July 2019

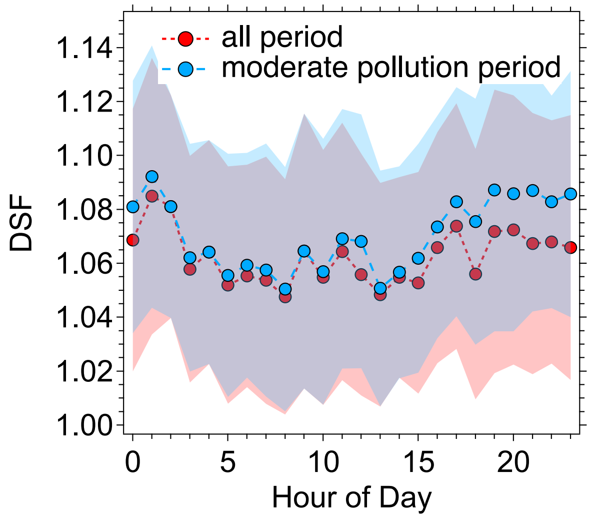

Figure 5 Diurnal variation in dynamic shape factor (χ) during the whole observation period and moderate pollution period ($35 < PM_{2.5} < 75$ μg/m^3)

https://doi.org/10.5194/acp-2019-433
Preprint. Discussion started: 1 July 2019

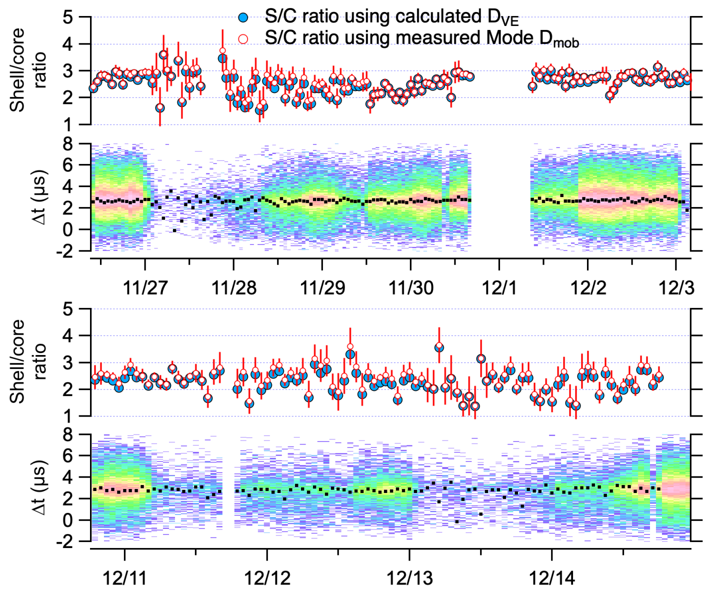

Figure 6 Temporal variations in shell/core ratio of rBC-containing particles calculated by both measured mode D_{mob} and derived D_{ve} and delay time distribution as a function of time.

https://doi.org/10.5194/acp-2019-433
Preprint. Discussion started: 1 July 2019

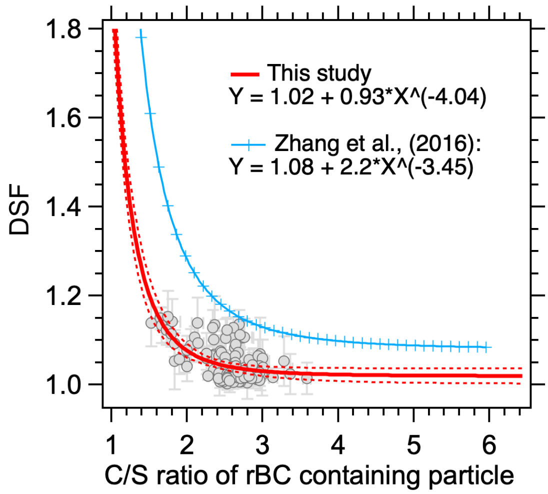

Figure 7 Dependence of χ value as a function of S/C ratio of rBC-containing particles during the observation period. Blue line with cross marks is the power function fitting result in the literature (Zhang et al., 2016). Red dotted lines are the upper and lower limits at a confidence interval of 90%.